Supplementary Information

Constraining aerosol deposition over the global ocean

Yipeng He‡*(1), David C. Kadko†(1), Mark P. Stephens (1), Michael T. Sheridan (2), Clifton S. Buck (2), Chris M. Marsay (3), William M. Landing (4), Minjie Zheng (5, 6), Pengfei Liu (7)

(1) Applied Research Center, Florida International University, Miami, Florida, 33174, USA

(2) Skidaway Institute of Oceanography, University of Georgia, Savannah, Georgia, 31411, USA

(3) School of Marine Science and Policy, University of Delaware, Newark, Delaware, 19711, USA

(4) Department of Earth, Ocean and Atmospheric Science, Florida State University, Tallahassee, Florida, 32306, USA

(5) Institute for Atmospheric and Climate Science, ETH Zürich, Zürich, Switzerland

(6) Department of Geology, Lund University, Lund, Sweden

(7) School of Earth and Atmospheric Sciences, Georgia Institute of Technology, Atlanta, Georgia, 30332, USA

‡ Present address: Marine Chemistry and Geochemistry, Woods Hole Oceanographic Institution, Woods Hole, Massachusetts, 02543, USA

†Deceased

*To Whom Correspondence Should be Addressed

Email: he.y@whoi.edu

Contents

Supplementary Texts S1. Preparation of iron impregnated acrylic fiber

The iron-impregnated acrylic fiber is widely used in the geosciences for the extraction of natural and cosmogenic radionuclides, such as ^{7}Be, ^{32}P and ^{234}Th from lake water, river water, and seawater[1, 2, 3, 4]. It is a cheap and easy technique to measure radionuclide activities in the aquatic environment for which typical concentrations of the target isotopes are extremely low. We have adopted a method from Krishnaswami et al.[1] and Lee et al.[3], and modified it for a better extraction efficiency. The modified procedure for preparing the fibers is as follows. Dissolve 3 kg of iron (III) chloride hexahydrate ($FeCl_3$•$(H_2O)_6$; ACS grade 97% assay; Fisher Chemical, Fisher Scientific Co.) into 20 L of deionized (DI) water. The solution is warmed and maintained at a temperature of 90°C with an immersion heater. Then 2 kg of acrylic fiber is added. The acrylic fiber is soaked in the hot solution for 30 min. In a fume hood, 2.5 L of ammonium hydroxide (NH_4OH; ACS grade 29.7% aqueous solution; Fisher Chemical, Fisher Scientific Co.) solution is diluted with 7.5 L of DI water. The fiber is removed from the $FeCl_3$ solution, wrung out, and transferred to the NH_4OH solution. After soaking for 2 hr, the acrylic fiber is removed from the solution and wrung out, then rinsed three times with at least 10 L of DI water. Afterwards, the fiber is spread out on a bench to air dry for several days. In order to shorten the drying time, it is recommended to turn and fluff the fibers daily to loosen clumps and create more surface area. When the fiber is completely dried, it is detangled and smoothed by use of a drum carder (Brother Drum Carder Inc.) and packed in zip lock bags (200 g per bag).

The extraction efficiency of iron impregnated acrylic fiber is tested for each batch. There are two ways to test the extraction efficiency: 1) using a stable ^{9}Be standard solution, or 2) placing two acrylic fiber cartridges in series.

For the ^{9}Be standard solution method, 500 ml of beryllium atomic absorption standard (1000 ppm) is added to a 500 L barrel containing seawater. The seawater is pumped through an acrylic fiber cartridge, and at every 100 L the cartridge effluent is collected for measurement of the Be content by atomic absorption spectroscopy. For the two filter cartridges in series method, 500 – 700 L of surface seawater is pumped through two acrylic fiber cartridges placed in series. After measuring the ^{7}Be extracted by each cartridge by gamma-ray spectroscopy, the extraction efficiency (e) can be calculated as:

$$e(\%) = \left(1 - \frac{^{7}Be_{2nd}}{^{7}Be_{1st}}\right) \times 100$$

where ${}^{7}Be_{1st}$ and ${}^{7}Be_{2nd}$ represent the ^{7}Be concentration of the first and the second fiber cartridge, respectively.

Supplementary References

1. Krishnaswami S, Lal D, Somayajulu BLK, Dixon FS, Stonecipher SA, Craig H. Silicon, radium, thorium, and lead in seawater: In-situ extraction by synthetic fibre. *Earth and Planetary Science Letters* 1972, **16**(1)**:** 84-90.

2. Lal D, Lee T. Cosmogenic 32P and 33P used as tracers to study phosphorus recycling in the upper ocean. *Nature* 1988, **333**(6175)**:** 752-754.

3. Lee T, Barg E, Lal D. Studies of vertical mixing in the Southern California Bight with cosmogenic radionuclides 32P and 7Be. *Limnology and Oceanography* 1991, **36**(5)**:** 1044-1052.

4. Kadko D, Olson D. Beryllium-7 as a tracer of surface water subduction and mixed-layer history. *Deep Sea Research Part I: Oceanographic Research Papers* 1996, **43**(2)**:** 89-116.

5. Gelaro R, McCarty W, Suárez MJ, Todling R, Molod A, Takacs L*, et al.* The Modern-Era Retrospective Analysis for Research and Applications, Version 2 (MERRA-2). *Journal of Climate* 2017, **30**(14)**:** 5419-5454.

6. Kadko D, Aguilar-Islas A, Bolt C, Buck CS, Fitzsimmons JN, Jensen LT*, et al.* The residence times of trace elements determined in the surface Arctic Ocean during the 2015 US Arctic GEOTRACES expedition. *Marine Chemistry* 2019, **208:** 56-69.

7. Kadko D, Landing WM, Shelley RU. A novel tracer technique to quantify the atmospheric flux of trace elements to remote ocean regions. *Journal of Geophysical Research: Oceans* 2015, **120**(2)**:** 848-858.

8. Kadko D, Landing WM, Buck CS. Quantifying Atmospheric Trace Element Deposition Over the Ocean on a Global Scale With Satellite Rainfall Products. *Geophysical Research Letters* 2020, **47**(7)**:** e2019GL086357.

9. Kadko D, Aguilar-Islas A, Buck CS, Fitzsimmons JN, Landing WM, Shiller A*, et al.* Sources, fluxes and residence times of trace elements measured during the U.S. GEOTRACES East Pacific Zonal Transect. *Marine Chemistry* 2020, **222:** 103781.

10. Zheng M, Liu H, Adolphi F, Muscheler R, Lu Z, Wu M*, et al.* Simulations of 7Be and 10Be with the GEOS-Chem global model v14.0.2 using state-of-the-art production rates. *Geoscientific Model Development* 2023, **16**(23)**:** 7037-7057.

11. Lal D, Peters B. Cosmic Ray Produced Radioactivity on the Earth. In: Sitte K (ed). *Kosmische Strahlung II / Cosmic Rays II*. Springer Berlin Heidelberg: Berlin, Heidelberg, 1967, pp 551-612.

12. Stein AF, Draxler RR, Rolph GD, Stunder BJB, Cohen MD, Ngan F. NOAA's HYSPLIT Atmospheric Transport and Dispersion Modeling System. *Bulletin of the American Meteorological Society* 2015, **96**(12)**:** 2059-2077.

Supplementary Table S1. Aerosol deployment information and measured aerosol ^{7}Be concentrations from the US GEOTRACES GP17-OCE cruise.

		Deployment Start			Deployment End							
Deploy#	GT#	Date[a]	Lat[b]	Lon[c]	Date[a]	Lat[b]	Lon[c]	Deploy Duration (hrs)	Vol Per Filter (m^3)	Aerosol ^{7}Be ± STD (dpm/m^3)	Mid Lat[b]	Mid Lon[c]
1	15904	12/3/22 04:42	-18.50	-150.60	12/5/22 04:14	-20.00	-152.00	17.6	97.3	0.1463 ± 0.0236	-20.00	-152.00
2	16129	12/7/22 01:17	-25.00	-151.25	12/9/22 01:29	-25.00	-151.25	26.5	147.4	0.0906 ± 0.0199	-25.00	-151.25
3	16251	12/9/22 03:33	-25.00	-151.25	12/10/22 23:20	-31.07	-150.25	18	102.2	0.1566 ± 0.0256	-27.92	-150.78
4	16354	12/11/22 02:35	-31.42	150.19	12/13/22 18:49	-36.73	-149.40	24	136.9	0.1609 ± 0.0229	-32.50	-150.00
5	16580	12/13/22 22:39	-37.48	-149.28	12/16/22 00:50	-39.33	-149.00	21.7	125.2	0.1896 ± 0.0229	-37.50	-149.28
6	16680	12/16/22 03:57	-39.93	-148.90	12/19/22 02:00	-46.33	-147.75	14.5	84.2	0.1208 ± 0.0269	-42.50	-148.47
7	16943	12/20/22 04:05	-47.54	-147.48	12/23/22 15:45	-52.31	-146.40	28.4	161.4	0.0241 ± 0.0164	-50.88	-146.75
8	17114	12/23/22 19:57	-52.31	-146.40	12/26/22 01:15	-55.01	-145.66	13.7	79.0	0.0003 ± 0.0281	-52.93	-146.24
9	17286	12/26/22 03:29	-55.01	-145.66	12/28/22 21:53	-56.30	-145.28	30.8	177.0	0.0695 ± 0.0173	-55.01	-145.67
10	17454	12/29/22 01:50	-56.30	-145.28	12/31/22 03:35	-57.60	-144.86	31.2	179.3	0.0734 ± 0.0153	-57.60	-144.86

11	17580	12/31/22 05:32	-57.60	-144.86	1/2/23 23:49	-60.00	-144.00	35.3	198.7	0.0867	±	0.0126	-59.39	-144.22
12	17769	1/3/23 21:07	-62.50	-143.00	1/6/23 16:01	-67.00	-135.00	13.5	77.3	0.1014	±	0.0249	-66.88	-135.26
13	17925	1/7/23 00:36	-67.01	-132.35	1/9/23 16:17	-66.99	-115.03	22	124.4	0.0220	±	0.0165	-66.99	-119.95
14	18117	1/10/23 19:07	-67.00	-114.77	1/15/23 15:56	-60.00	-82.50	9.3	51.3	0.0438	±	0.0483	-66.06	-96.40
15	18342	1/16/23 02:46	-60.00	-82.50	1/18/23 21:57	-55.00	-77.10	14.8	88.4	0.0632	±	0.0201	-58.02	-80.16
16	18428	1/19/23 00:11	-55.00	-77.10	1/22/23 01:20	-53.50	-75.75	26.5	153.6	0.1018	±	0.0167	-54.35	-76.55

Note: a) Date is recorded in UTC time zone; b) Latitude in North and South denoted as '+' and '-'; c) Longitude in East and West denoted as '+' and '-'.

Supplementary Table S2. Aerosol deployment information and measured aerosol ^{7}Be concentrations from the French GEOTRACES SWINGS GS02 cruise.

	Deployment Start			Deployment End							
Deploy#	Date[a]	Lat[b]	Lon[c]	Date[a]	Lat[b]	Lon[c]	Deploy Duration (hrs)	Vol Per Filter (m^3)	Aerosol ^{7}Be ± STD (dpm/m^3)	Mid Lat[b]	Mid Lon[c]
1	1/14/21 13:00	-25.00	51.00	1/15/21 9:31	-25.00	51.00	16.3	87.9	0.1851 ± 0.0092	-25.00	51.00
2	1/16/21 12:18	-27.17	44.46	1/16/21 12:10	-28.64	39.99	21.8	116.7	0.1155 ± 0.0142	-27.08	44.76
3	1/17/21 13:07	-28.64	39.99	1/18/21 12:28	-29.67	35.55	16.9	90.9	0.1815 ± 0.0212	-28.99	38.46
4	1/18/21 13:46	-29.75	35.19	1/19/21 20:06	-30.30	32.80	22.9	124.4	0.3701 ± 0.0231	-30.30	32.80
5	1/20/21 9:00	-29.80	31.70	1/22/21 13:07	-35.01	34.39	18.4	100.5	0.2813 ± 0.0249	-31.37	32.61
6	1/22/21 14:35	-35.22	34.47	1/24/21 12:27	-38.93	36.18	28.0	154.0	0.2801 ± 0.0133	-37.12	36.01
7	1/24/21 20:24	-39.80	36.37	1/28/21 6:35	-44.85	36.28	26.8	149.9	0.2735 ± 0.0172	-39.84	36.48
8	1/28/21 8:45	-44.89	36.24	1/30/21 18:11	-46.75	36.97	55.0	391.6	0.0890 ± 0.0015	-44.85	36.12
9	1/31/21 1:55	-47.16	37.64	2/2/21 10:56	-46.71	40.19	56.5	400.8	0.0464 ± 0.0037	-46.60	37.78
10	2/2/21 13:42	-46.75	41.05	2/4/21 13:30	-47.53	43.35	47.1	336.1	0.0897 ± 0.0021	-47.31	43.11

11	2/4/21 14:50	-47.84	43.70	2/8/21 5:10	-49.00	51.53	85.3	606.8	0.0600	±	0.0012	-52.05	49.37
12	2/8/21 6:48	-49.00	51.53	2/10/21 13:31	-45.11	52.03	54.5	390.7	0.1061	±	0.0015	-46.12	51.89
13	2/11/21 7:15	-46.84	55.37	2/13/21 9:35	-47.26	59.80	49.6	359.2	0.0912	±	0.0020	-47.08	56.42
14	2/15/21 6:16	-49.63	66.88	2/17/21 2:14	-52.70	74.72	43.8	314.0	0.0652	±	0.0022	-50.92	68.76
15	2/19/21 4:05	-54.17	73.65	2/21/21 9:08	-56.99	79.63	52.8	385.0	0.0603	±	0.0018	-55.54	76.89
16	2/21/21 11:02	-57.11	80.22	2/23/21 9:40	-57.99	81.48	46.7	327.9	0.0234	±	0.0097	-57.69	81.92
17	2/26/21 1:15	-53.02	72.63	2/28/21 1:35	-49.36	70.21	48.3	350.2	0.0735	±	0.0016	-51.19	73.37
18	2/28/21 6:45	-49.36	70.21	3/2/21 4:45	-45.00	67.80	45.7	326.1	0.0689	±	0.0022	-47.38	72.06
19	3/3/21 6:45	-39.24	64.64	3/4/21 11:17	-35.00	62.00	28.4	204.0	0.2439	±	0.0170	-36.42	62.93

Note: a) Date is recorded in UTC time zone; b) Latitude in North and South denoted as ‘+’ and ‘-’; c) Longitude in East and West denoted as ‘+’ and ‘-’.

Supplementary Table S3. Seawater sampling information, and seawater ^{7}Be concentrations and water column inventory at each sampling station for the US GEOTRACES GP17-OCE cruise.

Station	Date[a]	Lat[b]	Lon[c]	MLD[d]	Sample#	GT#	Depth	Seawater ^{7}Be ± STD (dpm/m^{3})			^{7}Be Inventory ± STD (dpm/m^{2})		
1	12/4/22	-20.00	-152.00	14	rr001	15992	14.7	415.7	±	17.1	30641	±	837
					rr002	15993	30.2	240.1	±	15.1			
					rr003	15994	50.2	230.9	±	13.0			
					rr004	15995	100.0	134.4	±	10.3			
					rr005	15996	124.9	117.1	±	8.7			
					rr006	15997	149.7	28.1	±	7.6			
3	12/7/22	-25.00	-151.25	20	rr007	16181	5.6	162.1	±	14.2	18057	±	720
					rr008	16182	25.1	165.5	±	13.8			
					rr009	16183	50.1	159.1	±	12.8			
					rr010	16184	79.5	146.8	±	8.6			
					rr011	16185	99.0	89.1	±	8.9			
					rr012	16186	123.7	40.1	±	8.1			
6	12/12/22	-32.50	-150.00	40	rr013	16430	33.0	321.4	±	21.9	29589	±	1346
					rr014	16431	72.8	131.2	±	14.7			
					rr015	16432	87.7	107.3	±	12.0			
					rr016	16433	102.3	88.9	±	10.4			
					rr017	16434	121.7	92.6	±	7.0			
					rr018	16435	140.9	88.2	±	7.5			
8	12/14/22	-37.50	-149.28	44	rr019	16621	20.2	326.0	±	18.8	26933	±	1089
					rr020	16622	60.1	167.9	±	8.7			
					rr021	16623	80.1	87.9	±	13.4			
					rr022	16624	99.9	80.7	±	10.2			
					rr023	16625	119.9	77.5	±	7.0			

					rr024	16626	139.8	50.6	±	6.3			
10	12/17/22	-42.50	-148.47	10	rr025	16780	10.3	330.4	±	23.2	24209	±	830
					rr026	16781	35.1	295.6	±	16.0			
					rr027	16782	54.9	111.2	±	12.8			
					rr028	16783	80.0	88.4	±	8.6			
					rr029	16784	104.9	68.4	±	9.0			
					rr030	16785	129.8	78.1	±	6.9			
12	12/19/22	-47.50	-147.52	38	rr031	16909	21.4	200.2	±	13.7	17743	±	887
					rr032	16910	61.3	72.3	±	13.1			
					rr033	16911	81.2	67.3	±	11.6			
					rr034	16912	101.2	45.3	±	12.8			
					rr035	16913	121.2	63.8	±	9.9			
					rr036	16914	141.2	69.0	±	7.5			
14	12/24/22	-52.31	-146.40	77	rr037	17141	33.9	137.5	±	18.5	14958	±	1523
					rr038	17142	78.1	85.4	±	12.8			
					rr039	17143	93.0	65.0	±	10.6			
					rr040	17144	107.5	39.5	±	9.8			
					rr041	17145	126.6	41.4	±	15.4			
					rr042	17146	146.1	32.5	±	8.6			
18	12/28/22	-56.30	-145.28	34	rr043	17405	30.8	70.7	±	8.7	10484	±	825
					rr044	17406	80.7	70.9	±	9.9			
					rr045	17407	115.7	37.8	±	11.0			
					rr046	17408	130.6	45.6	±	20.5			
					rr047	17409	145.4	37.0	±	10.0			
					rr048	17410	175.2	39.9	±	7.7			
20[e]	12/30/22	-57.60	-144.86	46	rr049	17534							

					rr050	17535	78.4	83.9	±	13.2			
					rr051	17536	108.5	94.3	±	11.2			
					rr052	17537	123.3	75.9	±	10.8			
					rr053	17538	143.4	58.8	±	11.9			
					rr054	17539	173.0	72.6	±	10.1			
22	1/2/23	-60.00	-144.00	58	rr055	17656	31.3	119.4	±	18.9	15280	±	1447
					rr056	17657	81.3	93.6	±	14.0			
					rr057	17658	96.4	87.8	±	11.2			
					rr058	17659	111.5	82.3	±	12.4			
					rr059	17660	131.4	45.6	±	12.3			
					rr060	17661	161.0	37.1	±	10.3			
25	1/5/23	-67.00	-135.00	18	rr061	17853	4.9	145.0	±	19.8	6184	±	870
					rr062	17854	24.8	41.5	±	12.9			
					rr063	17855	49.9	47.0	±	10.7			
					rr064	17856	79.9	3.8	±	11.8			
					rr065	17857	109.1	8.0	±	10.7			
					rr066	17858	139.8	17.0	±	10.7			
35	1/19/23	-54.35	-76.55	26	rr067	18479	17.5	159.0	±	16.4	18978	±	874
					rr068	18480	52.5	158.6	±	10.7			
					rr069	18481	72.5	143.6	±	7.5			
					rr070	18482	92.5	117.5	±	11.1			
					rr071	18483	112.4	61.5	±	12.8			
					rr072	18484	142.2	52.6	±	7.8			

Note: a) Date is recorded in UTC time zone; b) Latitude in North and South denoted as ‘+’ and ‘-’; c) Longitude in East and West denoted as ‘+’ and ‘-’; d) MLD denotes mixed layer depth, which is recognized from the temperature and salinity profile; e) Missing data due to a torn hose while pumping the seawater from the shallowest depth.

Supplementary Table S4. Seawater sampling station information, and seawater ^{7}Be concentrations and water column inventory at each sampling station for the French GEOTRACES SWINGS GS02 cruise.

Station	Date[a]	Lat[b]	Lon[c]	MLD[d]	Depth	Seawater ^{7}Be ± STD (dpm/m^3)			^{7}Be Inventory ± STD (dpm/m^2)		
7	1/21/21	-32.60	33.41	48	25.0	234.8	±	14.8	18243	±	1022
					40.0	225.9	±	13.1			
					60.0	90.6	±	9.9			
					80.0	88.8	±	9.7			
					100.0	55.9	±	8.3			
9	1/23/21	-37.08	36.02	30	30.0	549.2	±	22.4	34155	±	1416
					75.0	98.8	±	19.0			
					90.0	63.0	±	11.3			
					105.0	22.7	±	10.1			
					120.0	39.8	±	8.4			
11	1/26/21	-39.80	36.37	39	25.0	220.0	±	15.5	19708	±	1107
					65.0	100.7	±	14.9			
					80.0	75.5	±	10.8			
					95.0	92.6	±	27.3			
					115.0	61.9	±	8.8			
					135.0	53.4	±	9.8			
22	2/1/21	-47.50	39.30	39	45.0	261.0	±	17.5	27833	±	1381
					100.0	136.3	±	12.6			
					120.0	86.8	±	9.3			
25	2/4/21	-47.30	43.10	77	40.0	265.9	±	19.5	28698	±	1645
					95.0	187.7	±	16.5			
					115.0	82.2	±	10.2			
34	2/10/21	-45.00	52.00	35	30.0	369.1	±	21.0	28668	±	1300

					80.0	71.6	±	3.1				
					95.0	98.1	±	3.3				
					110.0	94.5	±	15.0				
					130.0	65.5	±	10.5				
					150.0	46.5	±	12.5				
38	2/13/21	-47.26	59.80	45	22.0	351.9	±	9.2		32272	±	1114
					60.0	261.9	±	21.4				
					85.0	97.3	±	17.1				
					110.0	75.5	±	18.4				
					135.0	80.6	±	13.2				
					156.0	75.2	±	16.8				
58	2/22/21	-57.69	81.92	55	5.0	168.9	±	20.9		13765	±	1860
					80.0	60.4	±	16.3				
					95.0	52.6	±	16.5				
64	2/25/21	-53.86	74.00	115	50.0	165.4	±	9.0		29075	±	1533
					110.0	236.4	±	25.7				
					125.0	99.2	±	11.9				
					140.0	115.1	±	8.1				
					150.0	77.2	±	10.3				
71	3/1/21	-45.00	67.80	25	15.0	444.9	±	28.2		43902	±	3647
					45.0	284.8	±	26.5				
					60.0	278.4	±	23.0				
					80.0	250.7	±	28.4				
73	3/3/21	-35.00	62.00	25	20.0	434.8	±	22.4		20273	±	1410
					55.0	77.7	±	12.1				
					70.0	60.1	±	17.9				

90.0	31.0	±	10.6	

Note: a) Date is recorded in UTC time zone; b) Latitude in North and South denoted as '+' and '-'; c) Longitude in East and West denoted as '+' and '-'; d) MLD denotes mixed layer depth, which is recognized from the temperature and salinity profile.

Supplementary Table S5. Upper ocean ^{7}Be inventories, ^{7}Be inferred effective bulk aerosol deposition velocities, and weighted precipitation rates from the Modern-Era Retrospective analysis for the Research and Applications Version 2 (MERRA-2)[5] for the US GEOTRACES GN01 cruise in the Arctic Ocean[6], the Bermuda Atlantic Series site (BATS) in North Atlantic[7], the US GEOTRACES GP15 cruise in the North and equatorial Pacific[8], the US GEOTRACES GP16 cruise in the eastern tropical Pacific[9], the US GEOTRACES GP17-OCE cruise (GP17) in the South Pacific and Southern Ocean (this study), and the French GEOTRACES GS02 cruise in South Indian Ocean (this study).

Cruise	Ocean Basin	Lat[a]	Lon[b]	^{7}Be Inventory (dpm/m^2)			Effective Bulk Aerosol Deposition (V_b; m/day)			Precipitation Rate (mm/day)
GN01	Arctic	75.84	-151.82	7400	±	1447	1190	±	233	0.48
BATS	North Atlantic	32.17	-64.50	37692	±	1582	2600	±	109	3.42
GP15	North and equatorial Pacific	54.70	-152.00	23386	±	994	1940	±	114	2.68
		53.70	-152.00	21523	±	751	1786	±	109	2.51
		52.00	-152.00	24750	±	1061	2053	±	143	2.49
		47.00	-152.00	25460	±	854	2112	±	131	2.88
		42.00	-152.00	22580	±	908	1873	±	107	1.35
		37.00	-152.00	22469	±	911	1864	±	128	1.84
		32.00	-152.00	22457	±	1348	1863	±	99	1.36
		27.00	-152.00	19979	±	1124	1657	±	113	1.16
		22.00	-152.00	15857	±	833	1316	±	106	1.65
		17.50	-152.00	21904	±	1188	1817	±	102	1.45
		11.00	-152.00	18240	±	669	3248	±	340	6.64
		7.50	-152.00	29830	±	1043	5312	±	505	10.09
		5.00	-152.00	28880	±	1070	5143	±	508	9.09
		2.50	-152.00	15551	±	766	1290	±	100	1.17
		-10.50	-152.00	16640	±	1074	1380	±	87	1.74

		-15.00	-152.00	21282	±	1207	1766	±	117	1.27
		-20.00	-152.00	22810	±	1403	1892	±	109	3.03
GP16	Equatorial Pacific	-12.00	-89.00	19666	±	819	1212	±	50	0.15
		-14.98	-112.75	12516	±	851	1223	±	83	0.12
		-14.00	-120.00	12930	±	1061	1264	±	104	0.16
		-11.67	-128.00	15085	±	1236	1474	±	121	0.26
		-11.58	-136.98	14906	±	1404	1457	±	137	1.15
		-11.03	-142.95	18258	±	1197	1785	±	117	3.39
		-10.77	-147.50	27230	±	949	2662	±	93	3.30
		-10.50	-152.00	34981	±	1124	3419	±	110	4.91
GP17	South Pacific Southern Ocean	-20.00	-152.00	30641	±	837	2723	±	148	3.81
		-25.00	-151.25	18057	±	720	1899	±	120	2.05
		-32.50	-150.00	29589	±	1346	2391	±	119	2.78
		-37.50	-149.28	26933	±	1089	1847	±	79	2.28
		-42.50	-148.47	24209	±	830	2028	±	111	1.89
		-47.50	-147.52	17743	±	887	1909	±	145	1.64
		-52.31	-146.40	14958	±	1523	1610	±	132	1.64
		-56.30	-145.28	10484	±	825	1909	±	154	1.89
		-60.00	-144.00	15280	±	1447	1959	±	173	1.72
		-67.00	-135.00	6184	±	870	1396	±	233	1.34
		-54.35	-76.55	18978	±	874	2425	±	138	3.45
GS02	South Indian Ocean	-37.08	36.02	34155	±	1416	3101	±	195	3.78
		-35.00	62.00	20273	±	1410	1841	±	155	2.48
		-39.80	36.37	19708	±	1107	1789	±	132	3.53
		-45.00	52.00	28668	±	1300	2603	±	170	3.05
		-47.26	59.80	32272	±	1114	2930	±	171	3.12
		-47.30	43.10	28698	±	1645	2605	±	194	3.09

-47.50	39.30	27833	±	1381	2527	±	173	3.21
-57.69	81.92	13765	±	1860	2433	±	333	2.98

Note: a) Latitude in North and South denoted as ‘+’ and ‘-’; b) Longitude in East and West denoted as ‘+’ and ‘-’.

Supplementary Table S6. The parameters and error associated probability distributions used in the microphysical size-fractionated aerosol ^{7}Be model and for the Monte Carlo simulation.

Parameter	Description	Value	Unit	Error	Probability Distribution	Ref.
η	A scale coefficient for the cosmogenic generated ^{7}Be	1.5915	μm^{-2}	5%	Normal	
ψ	Cosmogenic generated ^{7}Be rate	3.2E-03	dpm m^{-3} day^{-1}	5%	Lognormal	[10]
κ	A scale coefficient for the bulk aerosol deposition	1.16E-05	m^{-1}	5%	Normal	
θ	A scale coefficient for the washout rate	3.92E+05	μm^{-2}	5%	Normal	
ϕ	Aerosol size bin	0.1 – 10	μm			
λ	^{7}Be decay constant	0.013	Day^{-1}			[11]
PR	Precipitation rate	0 – 12	mm day^{-1}			

Supplementary Table S7. Uncertainties and sensitivities regarding the parameters used in the microphysical size-fractionated aerosol ^{7}Be model. The robustness of the aerosol ^{7}Be concentration (dpm/m^3) is tested based on 10,000 runs of a Monte Carlo simulation and summarized in three rows (from top to bottom: averaged value ± standard deviation, 50% confidence interval, 95% confidence interval) for each aerosol particle size from 0.1 – 10 μm.

Aerosol Particle Size (μm)	Precipitation Rate (mm/day)				
	0	3	6	9	12
0.1	4.32E-03 ± 3.40E-04	4.27E-03 ± 3.37E-04	4.23E-03 ± 3.33E-04	4.18E-03 ± 3.30E-04	4.13E-03 ± 3.27E-04
	4.09E-03 – 4.54E-03	4.04E-03 – 4.49E-03	4.00E-03 – 4.44E-03	3.95E-03 – 4.39E-03	3.91E-03 – 4.35E-03
	3.68E-03 – 5.01E-03	3.64E-03 – 4.96E-03	3.60E-03 – 4.90E-03	3.56E-03 – 4.85E-03	3.52E-03 – 4.79E-03
0.2	2.44E-02 ± 1.85E-03	2.29E-02 ± 1.75E-03	2.16E-02 ± 1.66E-03	2.04E-02 ± 1.59E-03	1.93E-02 ± 1.52E-03
	2.31E-02 – 2.56E-02	2.17E-02 – 2.40E-02	2.04E-02 – 2.26E-02	1.93E-02 – 2.14E-02	1.83E-02 – 2.03E-02
	2.09E-02 – 2.81E-02	1.96E-02 – 2.64E-02	1.84E-02 – 2.49E-02	1.74E-02 – 2.36E-02	1.65E-02 – 2.24E-02
0.3	6.22E-02 ± 4.66E-03	5.34E-02 ± 4.08E-03	4.67E-02 ± 3.66E-03	4.15E-02 ± 3.32E-03	3.74E-02 ± 3.05E-03
	5.90E-02 – 6.53E-02	5.06E-02 – 5.60E-02	4.42E-02 – 4.91E-02	3.93E-02 – 4.37E-02	3.53E-02 – 3.93E-02
	5.34E-02 – 7.16E-02	4.57E-02 – 6.16E-02	3.98E-02 – 5.41E-02	3.53E-02 – 4.83E-02	3.17E-02 – 4.36E-02
0.4	1.20E-01 ± 8.89E-03	9.08E-02 ± 7.03E-03	7.31E-02 ± 5.90E-03	6.12E-02 ± 5.09E-03	5.26E-02 ± 4.49E-03
	1.14E-01 – 1.26E-01	8.60E-02 – 9.53E-02	6.91E-02 – 7.69E-02	5.77E-02 – 6.45E-02	4.95E-02 – 5.55E-02
	1.03E-01 – 1.38E-01	7.75E-02 – 1.05E-01	6.20E-02 – 8.51E-02	5.16E-02 – 7.16E-02	4.42E-02 – 6.18E-02
0.5	1.99E-01 ± 1.46E-02	1.30E-01 ± 1.03E-02	9.65E-02 ± 8.07E-03	7.67E-02 ± 6.65E-03	6.37E-02 ± 5.66E-03
	1.89E-01 – 2.08E-01	1.23E-01 – 1.36E-01	9.09E-02 – 1.02E-01	7.21E-02 – 8.11E-02	5.98E-02 – 6.74E-02
	1.71E-01 – 2.28E-01	1.11E-01 – 1.51E-01	8.14E-02 – 1.13E-01	6.44E-02 – 9.04E-02	5.32E-02 – 7.55E-02
0.6	2.95E-01 ± 2.17E-02	1.65E-01 ± 1.34E-02	1.15E-01 ± 9.91E-03	8.79E-02 ± 7.86E-03	7.12E-02 ± 6.52E-03
	2.81E-01 – 3.10E-01	1.56E-01 – 1.74E-01	1.08E-01 – 1.21E-01	8.24E-02 – 9.29E-02	6.66E-02 – 7.54E-02
	2.55E-01 – 3.39E-01	1.40E-01 – 1.93E-01	9.63E-02 – 1.35E-01	7.33E-02 – 1.04E-01	5.92E-02 – 8.48E-02
0.7	4.12E-01 ± 3.02E-02	1.96E-01 ± 1.64E-02	1.29E-01 ± 1.15E-02	9.59E-02 ± 8.81E-03	7.64E-02 ± 7.15E-03

	3.91E-01	–	4.32E-01	1.85E-01	–	2.07E-01	1.21E-01	–	1.36E-01	8.98E-02	–	1.02E-01	7.14E-02	–	8.10E-02
	3.55E-01	–	4.73E-01	1.66E-01	–	2.30E-01	1.08E-01	–	1.53E-01	7.97E-02	–	1.14E-01	6.33E-02	–	9.15E-02
	5.54E-01	±	4.05E-02	2.24E-01	±	1.91E-02	1.40E-01	±	1.27E-02	1.02E-01	±	9.55E-03	8.03E-02	±	7.64E-03
0.8	5.27E-01	–	5.81E-01	2.11E-01	–	2.36E-01	1.31E-01	–	1.48E-01	9.54E-02	–	1.08E-01	7.50E-02	–	8.52E-02
	4.79E-01	–	6.37E-01	1.88E-01	–	2.63E-01	1.17E-01	–	1.67E-01	8.45E-02	–	1.22E-01	6.63E-02	–	9.63E-02
	7.12E-01	±	5.19E-02	2.46E-01	±	2.15E-02	1.49E-01	±	1.37E-02	1.06E-01	±	1.01E-02	8.29E-02	±	7.98E-03
0.9	6.77E-01	–	7.46E-01	2.31E-01	–	2.60E-01	1.39E-01	–	1.57E-01	9.94E-02	–	1.13E-01	7.74E-02	–	8.81E-02
	6.15E-01	–	8.17E-01	2.06E-01	–	2.90E-01	1.23E-01	–	1.77E-01	8.79E-02	–	1.28E-01	6.83E-02	–	9.98E-02
	8.96E-01	±	6.52E-02	2.64E-01	±	2.36E-02	1.55E-01	±	1.46E-02	1.10E-01	±	1.05E-02	8.50E-02	±	8.25E-03
1	8.52E-01	–	9.39E-01	2.48E-01	–	2.80E-01	1.45E-01	–	1.65E-01	1.02E-01	–	1.17E-01	7.92E-02	–	9.03E-02
	7.74E-01	–	1.03E+00	2.21E-01	–	3.13E-01	1.28E-01	–	1.86E-01	9.05E-02	–	1.32E-01	6.99E-02	–	1.02E-01
	1.31E+00	±	9.53E-02	2.92E-01	±	2.68E-02	1.64E-01	±	1.57E-02	1.14E-01	±	1.11E-02	8.76E-02	±	8.61E-03
2	1.25E+00	–	1.38E+00	2.73E-01	–	3.09E-01	1.53E-01	–	1.74E-01	1.07E-01	–	1.21E-01	8.16E-02	–	9.32E-02
	1.13E+00	–	1.51E+00	2.42E-01	–	3.48E-01	1.35E-01	–	1.97E-01	9.40E-02	–	1.38E-01	7.19E-02	–	1.06E-01
	1.82E+00	±	1.32E-01	3.11E-01	±	2.92E-02	1.70E-01	±	1.65E-02	1.17E-01	±	1.15E-02	8.93E-02	±	8.84E-03
3	1.73E+00	–	1.91E+00	2.91E-01	–	3.30E-01	1.59E-01	–	1.81E-01	1.09E-01	–	1.25E-01	8.31E-02	–	9.49E-02
	1.57E+00	–	2.09E+00	2.58E-01	–	3.73E-01	1.40E-01	–	2.05E-01	9.62E-02	–	1.42E-01	7.32E-02	–	1.08E-01
	2.41E+00	±	1.75E-01	3.25E-01	±	3.10E-02	1.74E-01	±	1.71E-02	1.19E-01	±	1.18E-02	9.04E-02	±	9.00E-03
4	2.29E+00	–	2.53E+00	3.03E-01	–	3.45E-01	1.62E-01	–	1.85E-01	1.11E-01	–	1.27E-01	8.41E-02	–	9.61E-02
	2.08E+00	–	2.77E+00	2.68E-01	–	3.90E-01	1.43E-01	–	2.10E-01	9.76E-02	–	1.44E-01	7.41E-02	–	1.09E-01
	3.09E+00	±	2.24E-01	3.35E-01	±	3.23E-02	1.77E-01	±	1.75E-02	1.20E-01	±	1.20E-02	9.11E-02	±	9.10E-03
5	2.94E+00	–	3.24E+00	3.12E-01	–	3.56E-01	1.65E-01	–	1.88E-01	1.12E-01	–	1.28E-01	8.48E-02	–	9.69E-02
	2.67E+00	–	3.54E+00	2.76E-01	–	4.03E-01	1.45E-01	–	2.14E-01	9.86E-02	–	1.46E-01	7.46E-02	–	1.10E-01
	3.80E+00	±	2.75E-01	3.42E-01	±	3.32E-02	1.79E-01	±	1.77E-02	1.21E-01	±	1.21E-02	9.16E-02	±	9.18E-03
6	3.61E+00	–	3.98E+00	3.19E-01	–	3.63E-01	1.67E-01	–	1.90E-01	1.13E-01	–	1.29E-01	8.52E-02	–	9.75E-02
	3.29E+00	–	4.36E+00	2.81E-01	–	4.12E-01	1.47E-01	–	2.17E-01	9.92E-02	–	1.47E-01	7.50E-02	–	1.11E-01

	8.56E+00	±	6.19E-01	3.60E-01	±	3.57E-02	1.84E-01	±	1.84E-02	1.23E-01	±	1.24E-02	9.29E-02	±	9.36E-03
7	8.14E+00	–	8.97E+00	3.35E-01	–	3.83E-01	1.71E-01	–	1.96E-01	1.15E-01	–	1.31E-01	8.64E-02	–	9.89E-02
	7.40E+00	–	9.81E+00	2.95E-01	–	4.36E-01	1.50E-01	–	2.23E-01	1.01E-01	–	1.50E-01	7.60E-02	–	1.13E-01
	1.45E+01	±	1.05E+00	3.66E-01	±	3.67E-02	1.85E-01	±	1.87E-02	1.24E-01	±	1.25E-02	9.33E-02	±	9.42E-03
8	1.38E+01	–	1.52E+01	3.41E-01	–	3.90E-01	1.72E-01	–	1.97E-01	1.15E-01	–	1.32E-01	8.67E-02	–	9.93E-02
	1.25E+01	–	1.67E+01	3.00E-01	–	4.44E-01	1.52E-01	–	2.25E-01	1.01E-01	–	1.51E-01	7.63E-02	–	1.13E-01
	2.12E+01	±	1.55E+00	3.69E-01	±	3.71E-02	1.86E-01	±	1.88E-02	1.24E-01	±	1.26E-02	9.35E-02	±	9.45E-03
9	2.02E+01	–	2.23E+01	3.43E-01	–	3.93E-01	1.73E-01	–	1.98E-01	1.16E-01	–	1.33E-01	8.69E-02	–	9.95E-02
	1.83E+01	–	2.44E+01	3.02E-01	–	4.48E-01	1.52E-01	–	2.26E-01	1.02E-01	–	1.51E-01	7.64E-02	–	1.14E-01
	4.25E+01	±	3.35E+00	3.72E-01	±	3.76E-02	1.87E-01	±	1.89E-02	1.25E-01	±	1.26E-02	9.37E-02	±	9.48E-03
10	4.02E+01	–	4.47E+01	3.46E-01	–	3.96E-01	1.74E-01	–	1.99E-01	1.16E-01	–	1.33E-01	8.71E-02	–	9.98E-02
	3.62E+01	–	4.93E+01	3.04E-01	–	4.52E-01	1.53E-01	–	2.27E-01	1.02E-01	–	1.52E-01	7.66E-02	–	1.14E-01

Supplementary Table S8. Uncertainties and sensitivities regarding the parameters used in the microphysical size-fractionated aerosol ^{7}Be model. The robustness of the effective bulk aerosol deposition velocity (m/day) is tested based on 10,000 runs of a Monte Carlo simulation and summarized in three rows (from top to bottom: averaged value ± standard deviation, 50% confidence interval, 95% confidence interval) for each aerosol particle size from 0.1 – 10 µm.

Aerosol Particle Size (µm)	Precipitation Rate (mm/day)				
	0	3	6	9	12
0.1	2.08E+03 ± 4.09E-12	2.11E+03 ± 1.86E+00	2.15E+03 ± 3.73E+00	2.19E+03 ± 5.59E+00	2.23E+03 ± 7.46E+00
	2.08E+03 – 2.08E+03	2.11E+03 – 2.12E+03	2.15E+03 – 2.15E+03	2.18E+03 – 2.19E+03	2.22E+03 – 2.23E+03
	2.08E+03 – 2.08E+03	2.11E+03 – 2.12E+03	2.14E+03 – 2.16E+03	2.18E+03 – 2.20E+03	2.21E+03 – 2.24E+03
0.2	1.15E+03 ± 2.02E-11	1.30E+03 ± 7.46E+00	1.44E+03 ± 1.49E+01	1.59E+03 ± 2.24E+01	1.74E+03 ± 2.98E+01
	1.15E+03 – 1.15E+03	1.29E+03 – 1.30E+03	1.43E+03 – 1.45E+03	1.58E+03 – 1.61E+03	1.72E+03 – 1.76E+03
	1.15E+03 – 1.15E+03	1.28E+03 – 1.31E+03	1.41E+03 – 1.47E+03	1.55E+03 – 1.63E+03	1.68E+03 – 1.80E+03
0.3	8.77E+02 ± 6.06E-11	1.21E+03 ± 1.68E+01	1.54E+03 ± 3.36E+01	1.88E+03 ± 5.04E+01	2.21E+03 ± 6.71E+01
	8.77E+02 – 8.77E+02	1.20E+03 – 1.22E+03	1.52E+03 – 1.57E+03	1.84E+03 – 1.91E+03	2.16E+03 – 2.25E+03
	8.77E+02 – 8.77E+02	1.18E+03 – 1.24E+03	1.48E+03 – 1.61E+03	1.78E+03 – 1.97E+03	2.08E+03 – 2.34E+03
0.4	7.24E+02 ± 2.96E-11	1.32E+03 ± 2.98E+01	1.91E+03 ± 5.97E+01	2.50E+03 ± 8.95E+01	3.09E+03 ± 1.19E+02
	7.24E+02 – 7.24E+02	1.30E+03 – 1.34E+03	1.87E+03 – 1.95E+03	2.44E+03 – 2.56E+03	3.01E+03 – 3.17E+03
	7.24E+02 – 7.24E+02	1.26E+03 – 1.37E+03	1.79E+03 – 2.02E+03	2.32E+03 – 2.67E+03	2.86E+03 – 3.32E+03
0.5	6.17E+02 ± 9.10E-13	1.54E+03 ± 4.66E+01	2.47E+03 ± 9.32E+01	3.39E+03 ± 1.40E+02	4.31E+03 ± 1.86E+02
	6.17E+02 – 6.17E+02	1.51E+03 – 1.57E+03	2.40E+03 – 2.53E+03	3.30E+03 – 3.48E+03	4.19E+03 – 4.44E+03
	6.17E+02 – 6.17E+02	1.45E+03 – 1.63E+03	2.28E+03 – 2.65E+03	3.12E+03 – 3.66E+03	3.95E+03 – 4.68E+03
0.6	5.63E+02 ± 3.30E-12	1.89E+03 ± 6.71E+01	3.22E+03 ± 1.34E+02	4.56E+03 ± 2.01E+02	5.89E+03 ± 2.69E+02
	5.63E+02 – 5.63E+02	1.85E+03 – 1.94E+03	3.13E+03 – 3.31E+03	4.42E+03 – 4.69E+03	5.71E+03 – 6.07E+03
	5.63E+02 – 5.63E+02	1.76E+03 – 2.03E+03	2.96E+03 – 3.49E+03	4.16E+03 – 4.95E+03	5.36E+03 – 6.41E+03
0.7	5.23E+02 ± 9.10E-12	2.33E+03 ± 9.14E+01	4.15E+03 ± 1.83E+02	5.96E+03 ± 2.74E+02	7.77E+03 ± 3.66E+02

	5.23E+02	–	5.23E+02	2.27E+03	–	2.40E+03	4.02E+03	–	4.27E+03	5.77E+03	–	6.14E+03	7.52E+03	–	8.01E+03
	5.23E+02	–	5.23E+02	2.15E+03	–	2.51E+03	3.79E+03	–	4.50E+03	5.42E+03	–	6.49E+03	7.05E+03	–	8.49E+03
	4.73E+02	±	1.61E-11	2.84E+03	±	1.19E+02	5.21E+03	±	2.39E+02	7.57E+03	±	3.58E+02	9.94E+03	±	4.77E+02
0.8	4.73E+02	–	4.73E+02	2.76E+03	–	2.92E+03	5.05E+03	–	5.37E+03	7.33E+03	–	7.81E+03	9.62E+03	–	1.03E+04
	4.73E+02	–	4.73E+02	2.61E+03	–	3.07E+03	4.74E+03	–	5.67E+03	6.87E+03	–	8.27E+03	9.00E+03	–	1.09E+04
	4.50E+02	±	1.01E-11	3.44E+03	±	1.51E+02	6.44E+03	±	3.02E+02	9.43E+03	±	4.53E+02	1.24E+04	±	6.04E+02
0.9	4.50E+02	–	4.50E+02	3.34E+03	–	3.55E+03	6.24E+03	–	6.64E+03	9.13E+03	–	9.74E+03	1.20E+04	–	1.28E+04
	4.50E+02	–	4.50E+02	3.15E+03	–	3.74E+03	5.85E+03	–	7.03E+03	8.54E+03	–	1.03E+04	1.12E+04	–	1.36E+04
	4.20E+02	±	3.18E-12	4.12E+03	±	1.86E+02	7.81E+03	±	3.73E+02	1.15E+04	±	5.59E+02	1.52E+04	±	7.46E+02
1	4.20E+02	–	4.20E+02	3.99E+03	–	4.24E+03	7.56E+03	–	8.06E+03	1.11E+04	–	1.19E+04	1.47E+04	–	1.57E+04
	4.20E+02	–	4.20E+02	3.75E+03	–	4.48E+03	7.08E+03	–	8.54E+03	1.04E+04	–	1.26E+04	1.37E+04	–	1.67E+04
	3.94E+02	±	7.62E-12	5.72E+03	±	2.69E+02	1.10E+04	±	5.37E+02	1.64E+04	±	8.06E+02	2.17E+04	±	1.07E+03
2	3.94E+02	–	3.94E+02	5.54E+03	–	5.90E+03	1.07E+04	–	1.14E+04	1.58E+04	–	1.69E+04	2.10E+04	–	2.24E+04
	3.94E+02	–	3.94E+02	5.19E+03	–	6.24E+03	9.99E+03	–	1.21E+04	1.48E+04	–	1.79E+04	1.96E+04	–	2.38E+04
	3.66E+02	±	1.74E-11	7.61E+03	±	3.66E+02	1.49E+04	±	7.31E+02	2.21E+04	±	1.10E+03	2.93E+04	±	1.46E+03
3	3.66E+02	–	3.66E+02	7.37E+03	–	7.86E+03	1.44E+04	–	1.53E+04	2.14E+04	–	2.28E+04	2.84E+04	–	3.03E+04
	3.66E+02	–	3.66E+02	6.90E+03	–	8.33E+03	1.34E+04	–	1.63E+04	2.00E+04	–	2.43E+04	2.65E+04	–	3.22E+04
	3.45E+02	±	6.42E-12	9.81E+03	±	4.77E+02	1.93E+04	±	9.55E+02	2.87E+04	±	1.43E+03	3.82E+04	±	1.91E+03
4	3.45E+02	–	3.45E+02	9.49E+03	–	1.01E+04	1.86E+04	–	1.99E+04	2.78E+04	–	2.97E+04	3.69E+04	–	3.95E+04
	3.45E+02	–	3.45E+02	8.87E+03	–	1.07E+04	1.74E+04	–	2.11E+04	2.59E+04	–	3.15E+04	3.45E+04	–	4.19E+04
	3.27E+02	±	2.96E-12	1.23E+04	±	6.04E+02	2.43E+04	±	1.21E+03	3.63E+04	±	1.81E+03	4.82E+04	±	2.42E+03
5	3.27E+02	–	3.27E+02	1.19E+04	–	1.27E+04	2.35E+04	–	2.51E+04	3.50E+04	–	3.75E+04	4.66E+04	–	4.99E+04
	3.27E+02	–	3.27E+02	1.11E+04	–	1.35E+04	2.19E+04	–	2.67E+04	3.27E+04	–	3.98E+04	4.35E+04	–	5.30E+04
	3.32E+02	±	7.84E-12	1.51E+04	±	7.46E+02	2.99E+04	±	1.49E+03	4.47E+04	±	2.24E+03	5.95E+04	±	2.98E+03
6	3.32E+02	–	3.32E+02	1.46E+04	–	1.56E+04	2.89E+04	–	3.09E+04	4.32E+04	–	4.62E+04	5.75E+04	–	6.15E+04
	3.32E+02	–	3.32E+02	1.37E+04	–	1.66E+04	2.70E+04	–	3.28E+04	4.03E+04	–	4.91E+04	5.36E+04	–	6.53E+04

	3.31E+02	±	1.37E-11	3.36E+04	±	1.68E+03	6.69E+04	±	3.36E+03	1.00E+05	±	5.04E+03	1.33E+05	±	6.71E+03
7	3.31E+02	–	3.31E+02	3.25E+04	–	3.47E+04	6.46E+04	–	6.91E+04	9.68E+04	–	1.04E+05	1.29E+05	–	1.38E+05
	3.31E+02	–	3.31E+02	3.03E+04	–	3.69E+04	6.03E+04	–	7.35E+04	9.03E+04	–	1.10E+05	1.20E+05	–	1.47E+05
	4.01E+02	±	6.14E-12	5.96E+04	±	2.98E+03	1.19E+05	±	5.97E+03	1.78E+05	±	8.95E+03	2.37E+05	±	1.19E+04
8	4.01E+02	–	4.01E+02	5.76E+04	–	6.15E+04	1.15E+05	–	1.23E+05	1.72E+05	–	1.84E+05	2.29E+05	–	2.45E+05
	4.01E+02	–	4.01E+02	5.37E+04	–	6.54E+04	1.07E+05	–	1.30E+05	1.60E+05	–	1.95E+05	2.14E+05	–	2.60E+05
	5.04E+02	±	8.41E-12	9.29E+04	±	4.66E+03	1.85E+05	±	9.32E+03	2.78E+05	±	1.40E+04	3.70E+05	±	1.86E+04
9	5.04E+02	–	5.04E+02	8.98E+04	–	9.60E+04	1.79E+05	–	1.92E+05	2.68E+05	–	2.87E+05	3.58E+05	–	3.83E+05
	5.04E+02	–	5.04E+02	8.38E+04	–	1.02E+05	1.67E+05	–	2.04E+05	2.50E+05	–	3.05E+05	3.34E+05	–	4.07E+05
	2.13E+03	±	2.32E-11	3.72E+05	±	1.86E+04	7.42E+05	±	3.73E+04	1.11E+06	±	5.59E+04	1.48E+06	±	7.46E+04
10	2.13E+03	–	2.13E+03	3.59E+05	–	3.84E+05	7.17E+05	–	7.66E+05	1.07E+06	–	1.15E+06	1.43E+06	–	1.53E+06
	2.13E+03	–	2.13E+03	3.35E+05	–	4.08E+05	6.68E+05	–	8.15E+05	1.00E+06	–	1.22E+06	1.33E+06	–	1.63E+06

Supplementary Table S9. Effective bulk aerosol deposition velocity derived from the GEOS-Chem model and ^{7}Be measurements over global oceans and their relative differences ($V_{GEOS-Chem}/V_{7Be} - 1$) are summarized in three rows (from top to bottom: GEOS-Chem model, ^{7}Be measurements, relative differences) for each ocean basin.

Ocean Basin	Year Averaged	# of Data	Mean	Std	Min	Max	Median	Unit
			1733	712	144	4336	1671	m/day
North Pacific	2013-2023	1957	2752	913	1179	6825	2611	m/day
			-37.1	16.6	-88.0	0.1	-33.4	%
			1880	679	250	5039	1982	m/day
South Pacific	2013-2023	2190	2363	773	1188	7151	2321	m/day
			-20.9	17.8	-80.9	20.6	-15.7	%
			1312	512	83	2579	1400	m/day
North Atlantic	2013-2023	1322	2215	585	1112	5071	2157	m/day
			-41.8	17.4	-92.6	-17.6	-38.1	%
			1482	591	141	2323	1616	m/day
South Atlantic	2013-2023	1051	2043	525	1140	4736	2123	m/day
			-30.0	18.2	-87.8	1.3	-23.9	%
			1541	556	145	3690	1550	m/day
Indian Ocean	2013-2023	1770	2366	686	1177	6360	2331	m/day
			-33.6	21.9	-87.9	-0.7	-28.9	%
			477	189	211	1394	428	m/day
Arctic Ocean	2013-2023	1161	1462	134	1277	2088	1418	m/day
			-68.1	8.8	-83.5	-31.3	-69.9	%
			865	442	109	1958	810	m/day
Southern Ocean	2013-2023	1033	1941	274	1230	2781	1983	m/day
			-57.5	17.7	-91.2	-15.0	-59.0	%
			1422	730	83	5039	1444	m/day
Global Oceans	2013-2023	10484	2234	752	1112	7151	2161	m/day
			-38.6	22.9	-92.6	20.6	-34.7	%

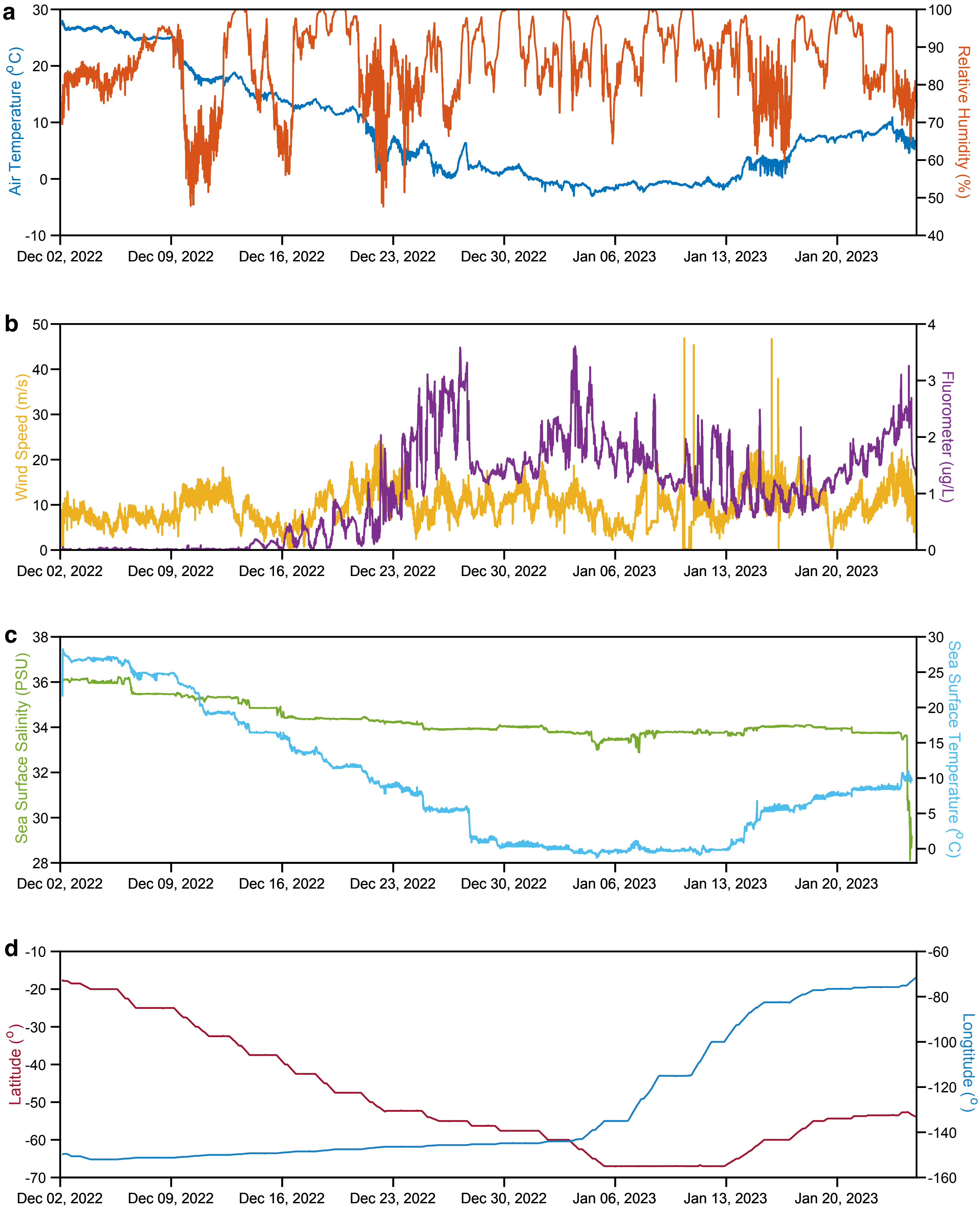

Supplementary Figure S1

Supplementary Figure S1. Underway data of atmosphere and surface seawater parameters by ship-equipped instruments from the US GEOTRACES GP17-OCE cruise (i.e. air temperature, relative humidity, wind speed, fluorometer, sea surface temperature and salinity).

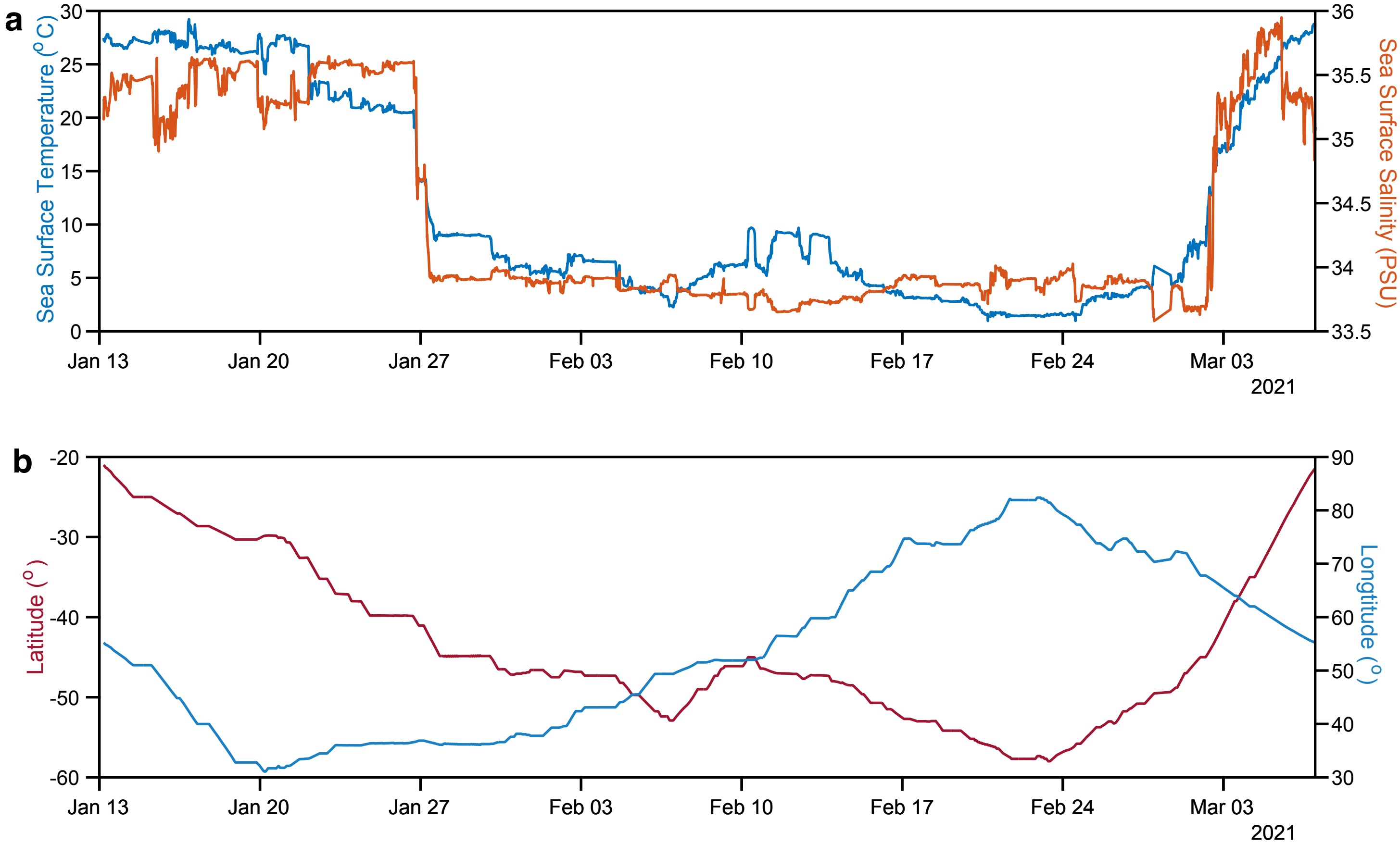

Supplementary Figure S2. Underway surface seawater parameters by ship-equipped instruments from the French GEOTRACES GS02 cruise (i.e. sea surface temperature and salinity).

Supplementary Figure S2

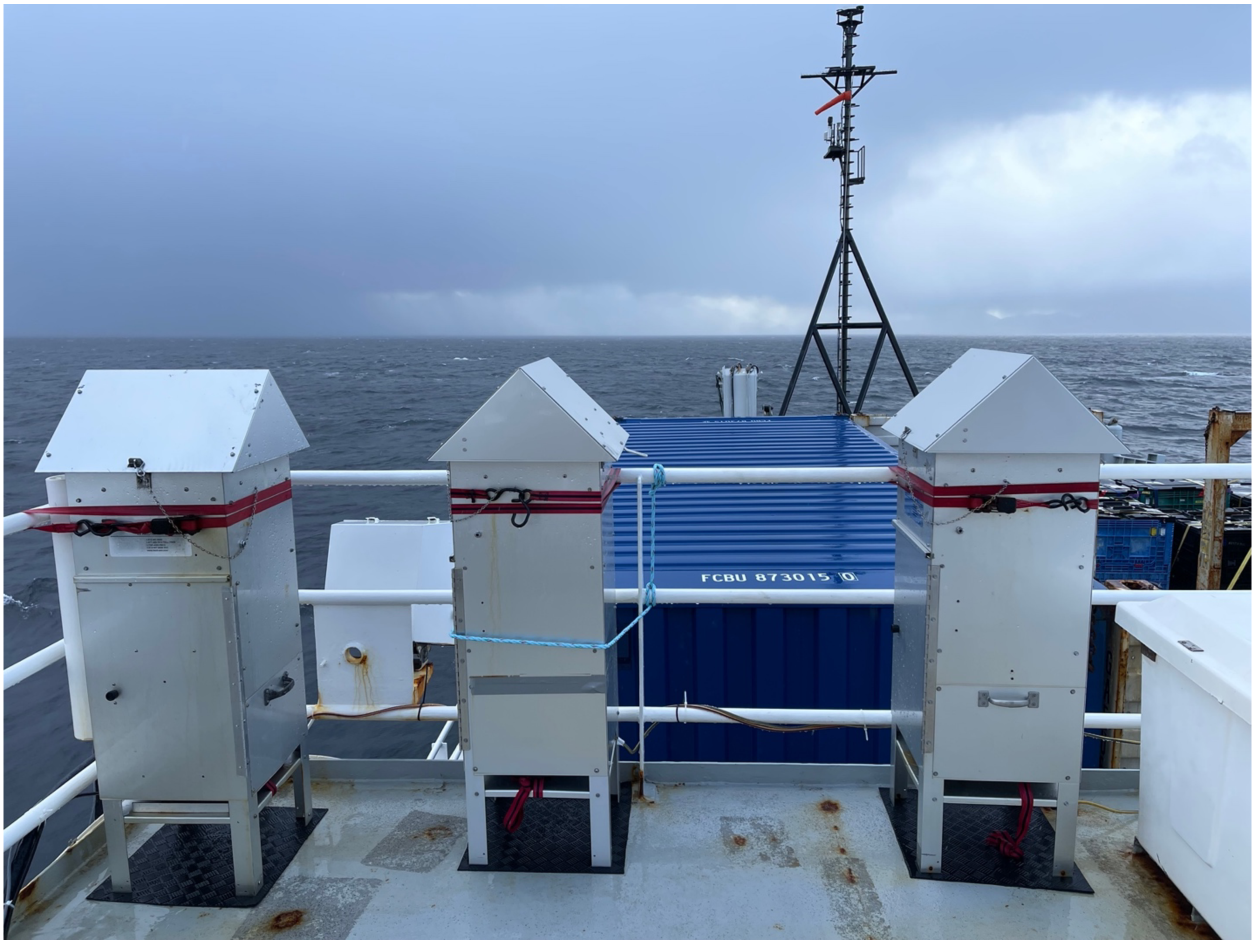

Supplementary Figure S3. A photo of the high-volume aerosol samplers on the front rail of the 03 deck of the R/V *Roger Revelle*.

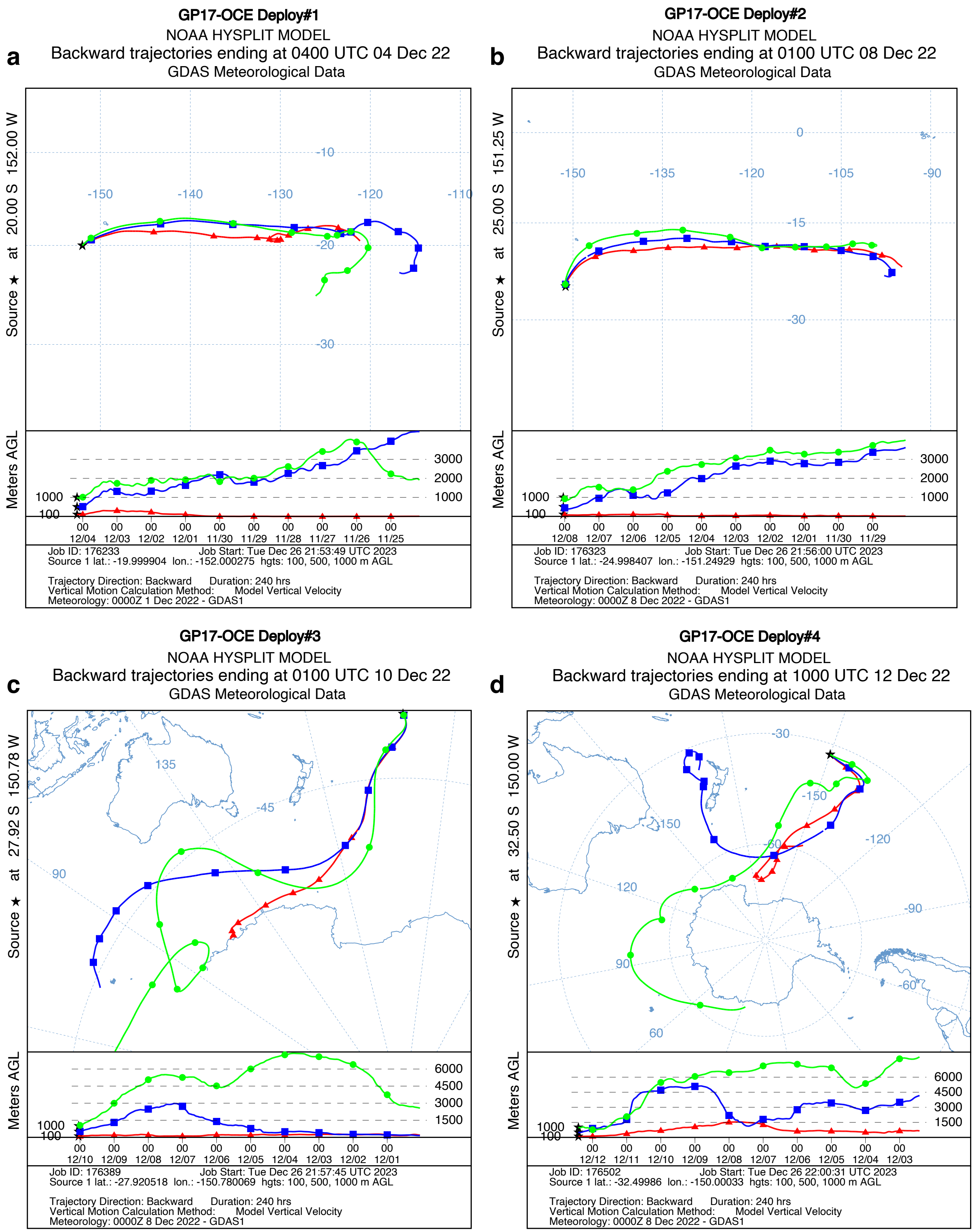

Supplementary Figure S4

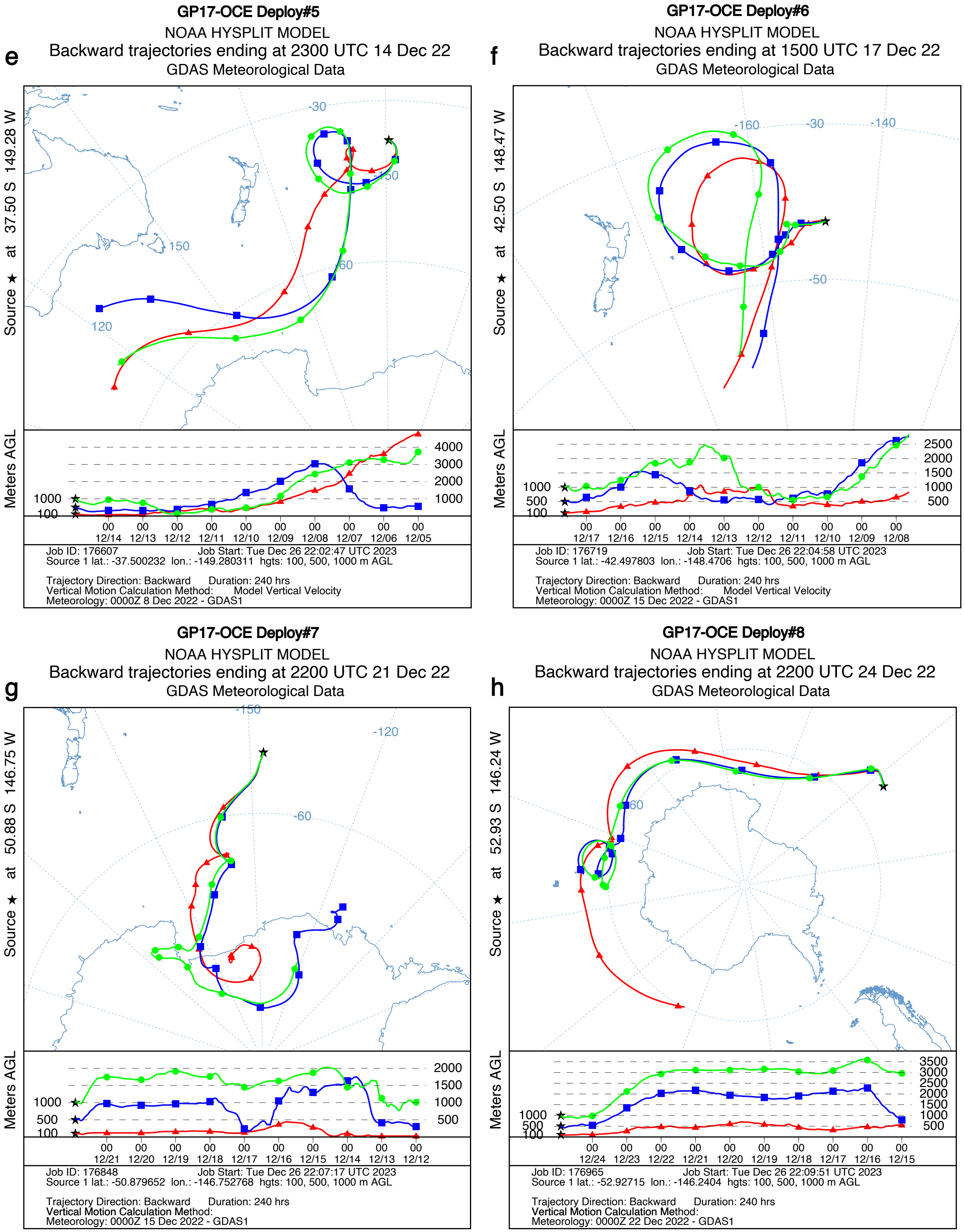

SupplementaryFigureS4 (Continued)

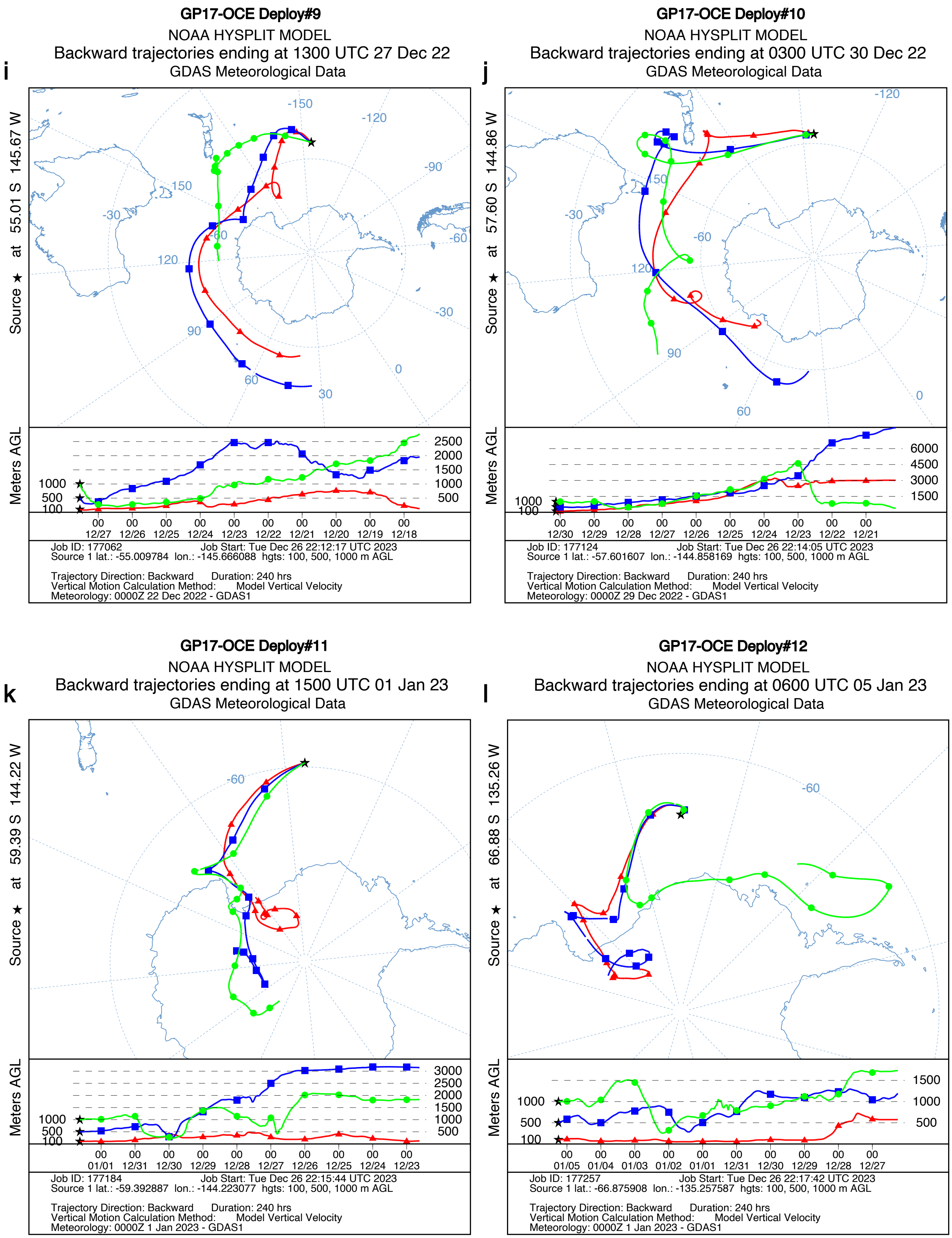

SupplementaryFigureS4 (Continued)

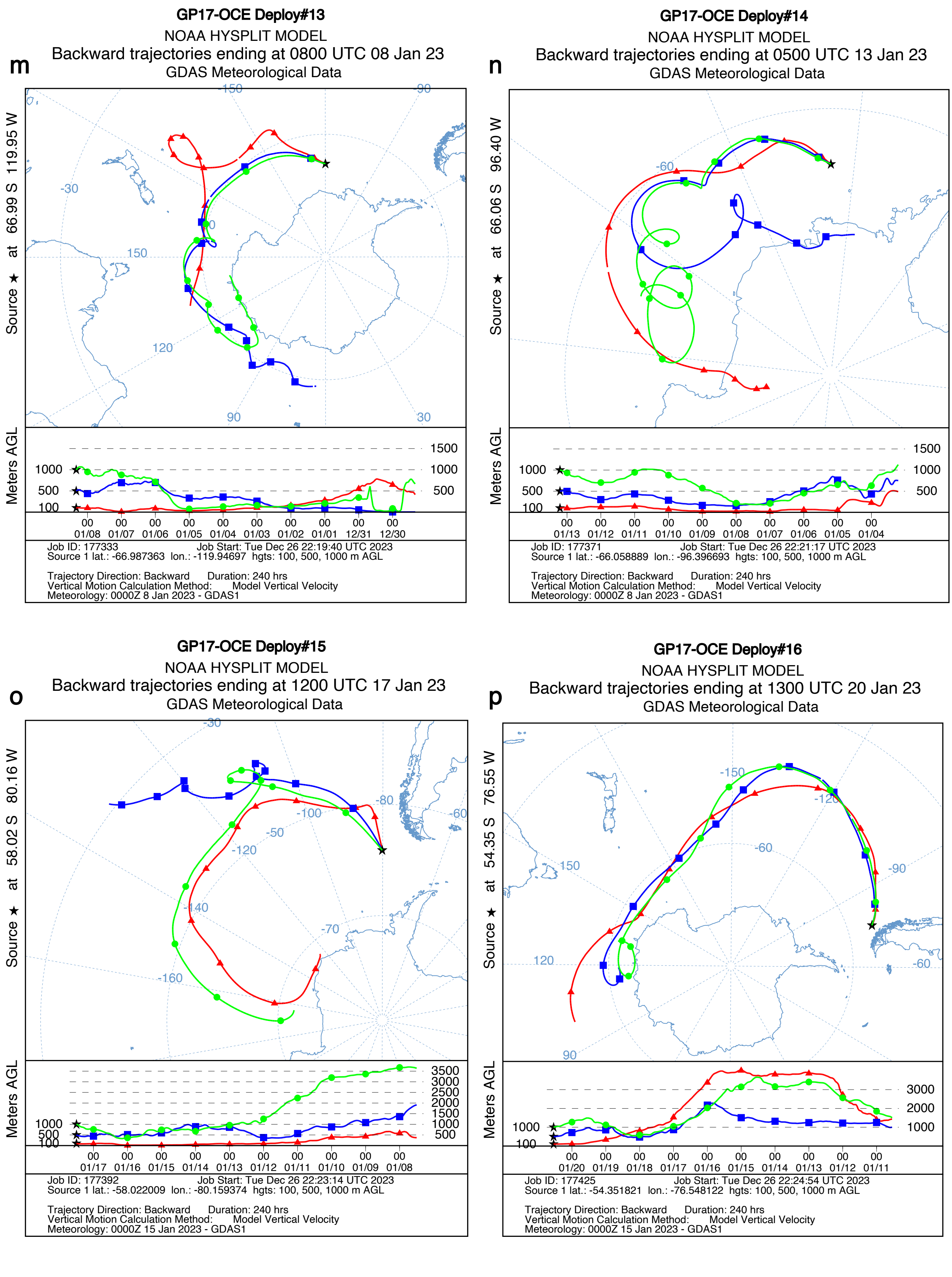

Supplementary Figure S4 (Continued)

Supplementary Figure S4. 10-day air mass back trajectory analysis using the HYSPLIT model[12] for each aerosol sampling event conducted during the GP17 cruise.

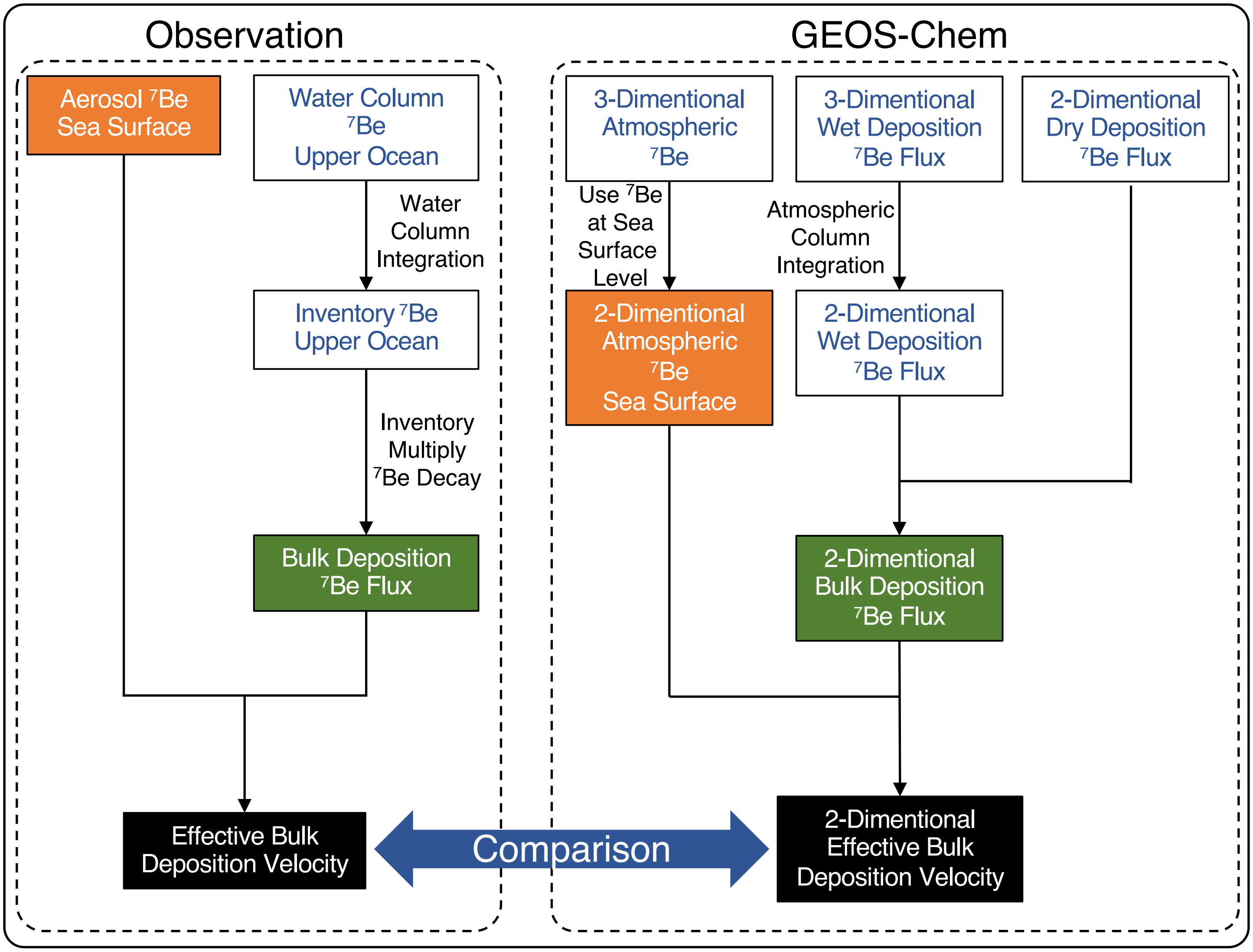

Supplementary Figure S5. A schematic flowchart of the procedures for calculating and comparing the effective bulk deposition velocities from both GEOS-Chem and our observational data set.

Supplementary Figure S5

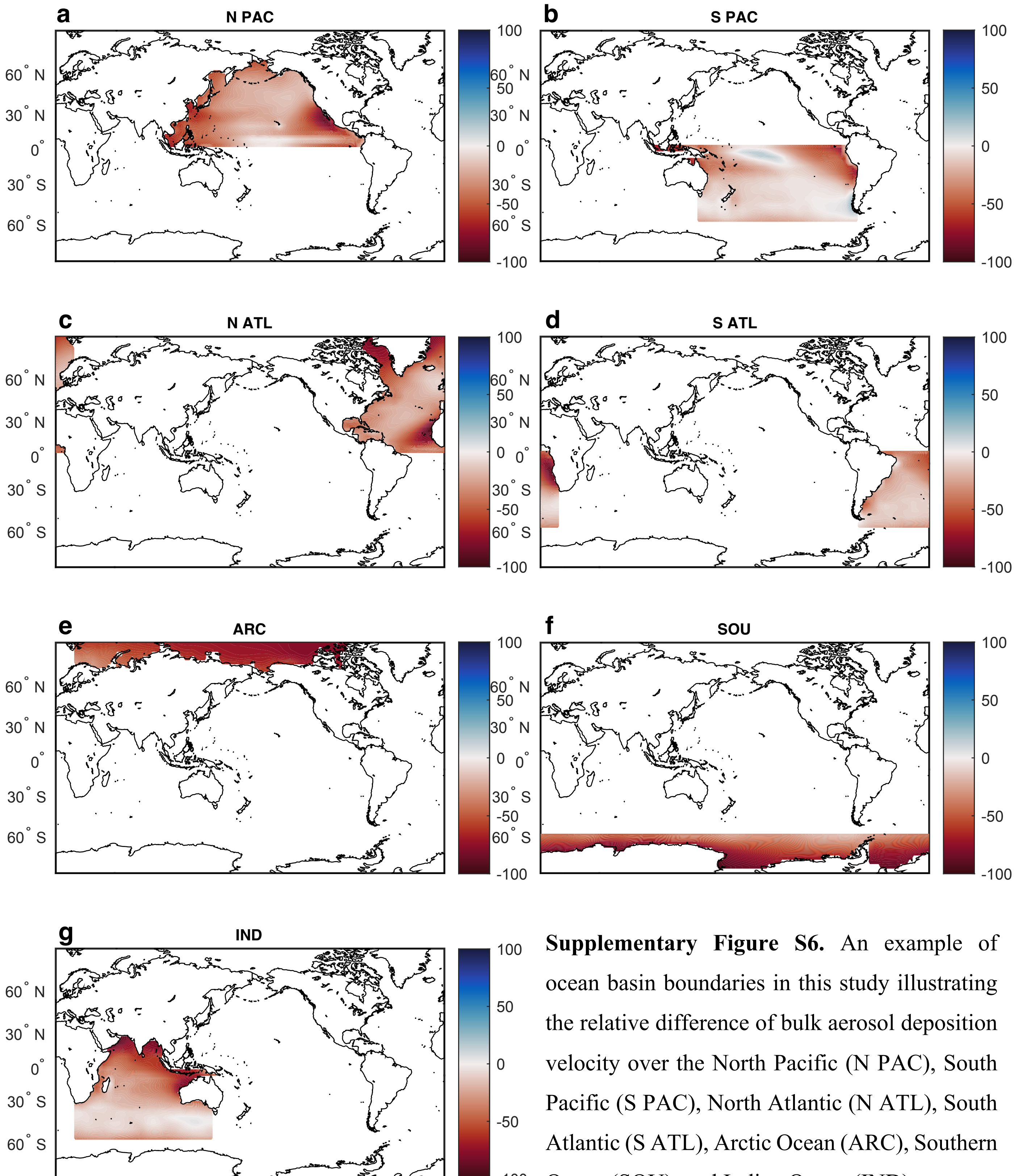

Supplementary Figure S6. An example of ocean basin boundaries in this study illustrating the relative difference of bulk aerosol deposition velocity over the North Pacific (N PAC), South Pacific (S PAC), North Atlantic (N ATL), South Atlantic (S ATL), Arctic Ocean (ARC), Southern Ocean (SOU), and Indian Ocean (IND).

Supplementary Figure S6

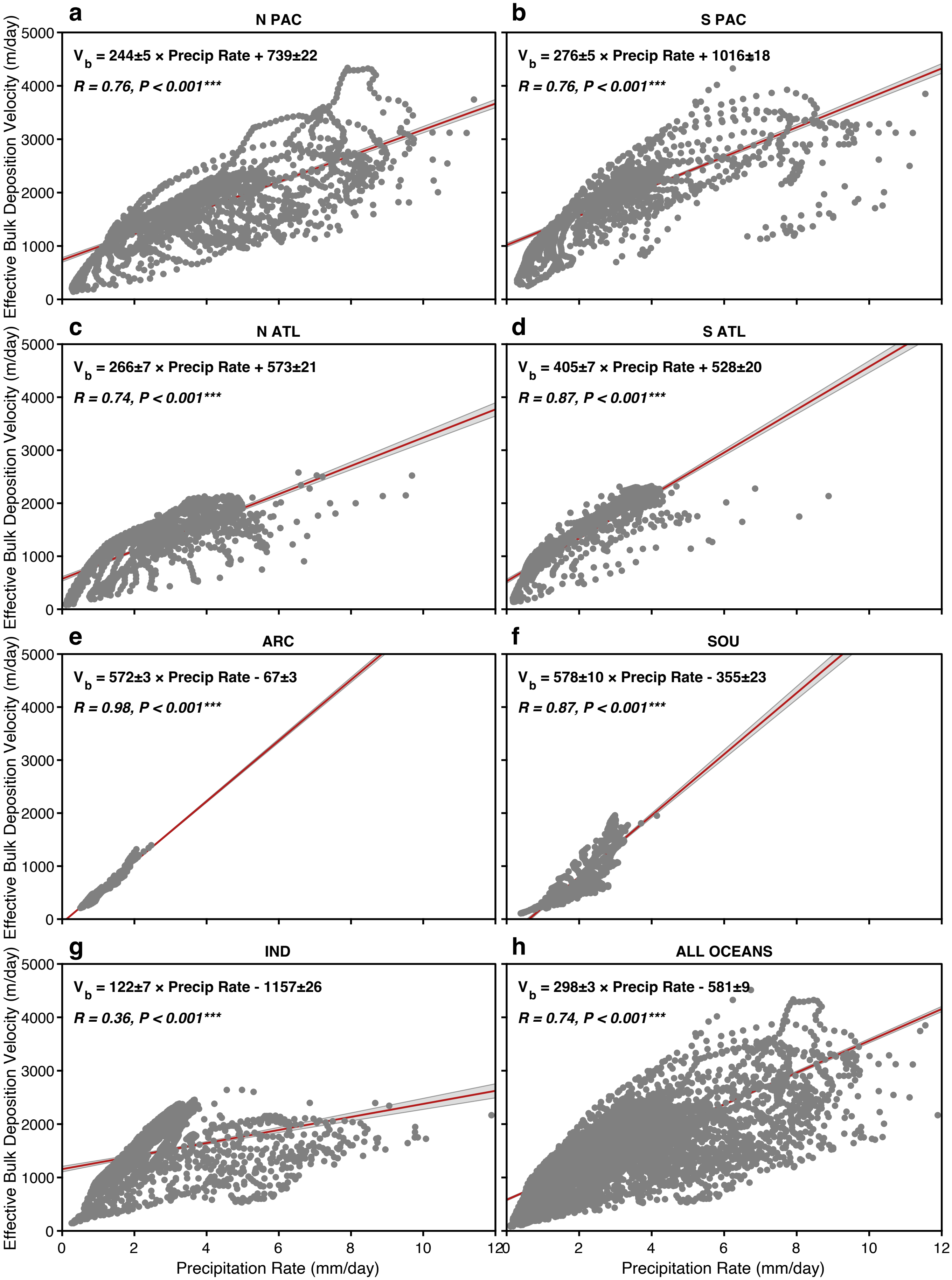

Supplementary Figure S7

Supplementary Figure S7. The linear correlation between effective bulk aerosol deposition velocity and precipitation rate for the GEOS-Chem simulation results over the North Pacific (N PAC), South Pacific (S PAC), North Atlantic (N ATL), South Atlantic (S ATL), Arctic Ocean (ARC), Southern Ocean (SOU), and Indian Ocean (IND). Robustness is denoted as *Pearson's R* and significance levels are denoted as *** ($p < 0.001$), ** ($p < 0.01$), and * ($p < 0.05$). The intercept of the linear correlation implies that dry deposition velocity for the aerosol over the ocean surface, in the absence of precipitation.

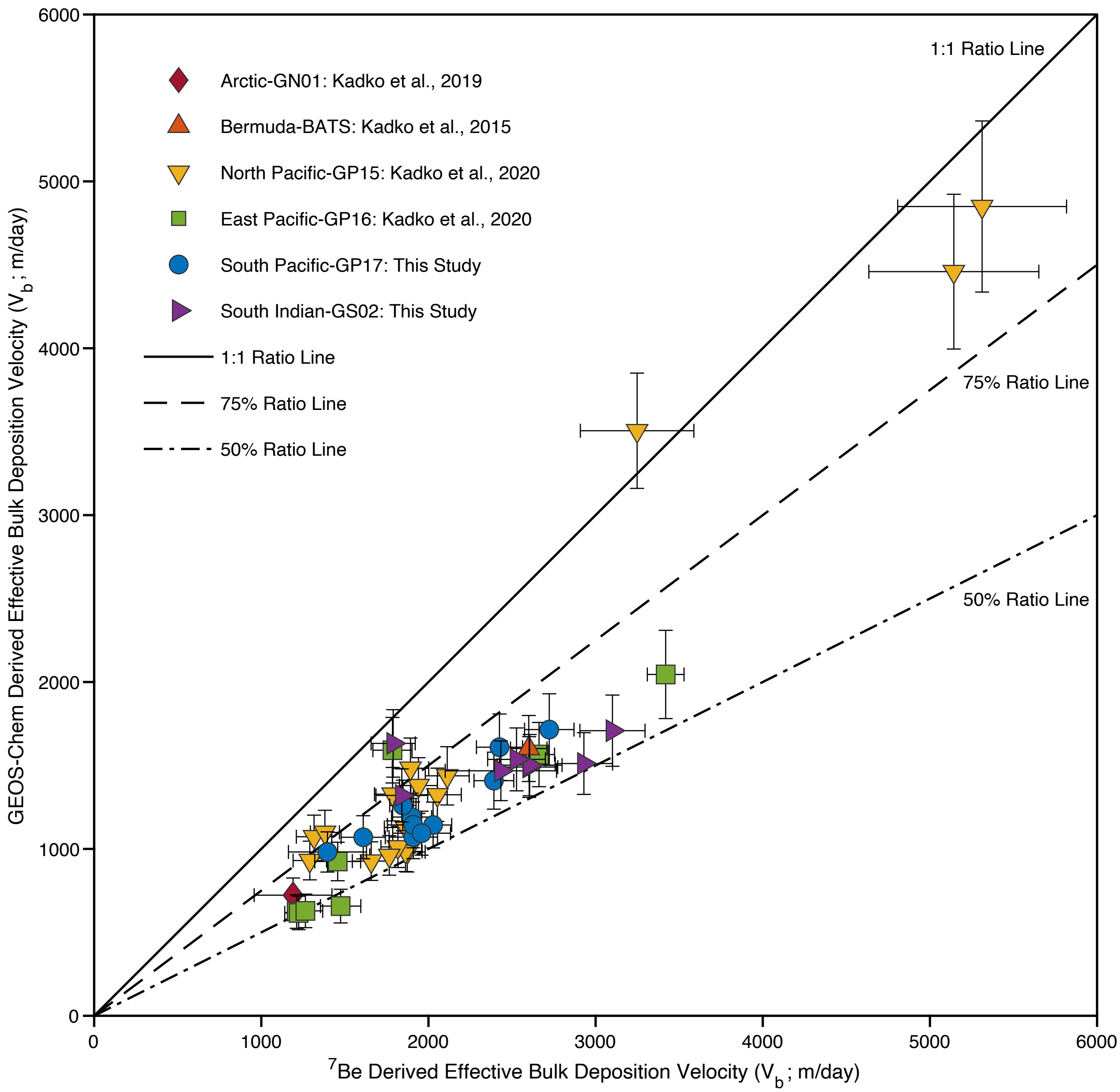

Supplementary Figure S8. Site-by-site comparison of effective bulk aerosol deposition velocities inferred from ^{7}Be measurements versus those derived from the GEOS-Chem model over global oceans. ^{7}Be-based measurements are shown for Arctic-GN01 (red diamonds), Bermuda-BATS (orange upward triangles), North Pacific-GP15 (yellow downward triangles), East Pacific-GP16 (green squares), South Pacific-GP17 (blue circles), and South Indian-GS02 (purple rightward triangles). The 1:1 line, along with 75% and 50% ratio lines, are included to illustrate the degree of agreement between observationally derived and modeled deposition velocities.

Supplementary Figure S8